Thermodynamic stability of a spin microemulsion in Rashba spin-orbit-coupled bosons

Ethan C. McGarrigle, Ron Nodel, Kris T. Delaney, Leon Balents, and Glenn H. Fredrickson

Phys. Rev. A **110**, L041303 — Published 24 October 2024

DOI: 10.1103/PhysRevA.110.L041303

Thermodynamic stability of a spin microemulsion in Rashba spin-orbit coupled bosons

Ethan C. McGarrigle,[1] Ron Nodel,[2] Kris T. Delaney,[3] Leon Balents,[4,5] and Glenn H. Fredrickson[1,3,6,*]

[1] *Department of Chemical Engineering, University of California, Santa Barbara, 93106, California, USA*
[2] *Department of Physics, University of California, Santa Barbara, 93106, California, USA*
[3] *Materials Research Laboratory, University of California, Santa Barbara, 93106, California, USA*
[4] *Kavli Institute for Theoretical Physics, University of California, Santa Barbara, 93106, California, USA*
[5] *Canadian Institute for Advanced Research, Toronto, Ontario M5G 1M1, Canada*
[6] *Materials Department, University of California, Santa Barbara, 93106, California, USA*

Recent finite-temperature numerical simulations have unveiled a quantum "spin" microemulsion analogue, found by raising the temperature of a stripe supersolid phase in a Rashba spin-orbit coupled Bose gas. This microemulsion state is a highly-correlated, isotropic normal fluid where atoms self-arrange based on their internal pseudospin into patterns that resemble bicontinuous microemulsions. This finding leaves several open questions regarding the broader accessibility of this phase in experiments. Here, we use equilibrium finite-temperature numerical simulations based on a coherent state path integral representation to perform a computational investigation into the thermodynamic stability of the spin microemulsion state. Numerical simulations emphasize the requirement of a nearly, but not perfectly, isotropic spin-orbit coupling in order to achieve the microemulsion phase in cold-atom experiments. Moreover, the microemulsion state exists independent of miscibility of the pseudospin components and for a wide range of pseudospin population imbalance, suggesting a high degree of flexibility in choosing the atom and hyperfine states in an experimental realization. Finally, we demonstrate this feasibility by mimicking a Rashba spin-orbit coupled ^{87}Rb experiment in an isotropic harmonic trap, where we confirm the microemulsion's existence via its density profile and equilibrium quasi-momentum distribution.

I. INTRODUCTION

The growing field of quantum liquid crystals describes quantum mechanical systems that possess the mesoscopic ordered textures of classical smectic and nematic liquid crystals. Examples include stripe, charge density wave, and Wigner crystalline states found in electronic systems [1–4] as well as stripe phases found in dipolar and spin-orbit coupled cold atom systems [5, 6]. Within the quantum liquid crystal paradigm, quantum "microemulsion" phases were first proposed years ago by Kivelson and Spivak [7, 8] as intermediates between Wigner crystals and 2D electron gases in metal-oxide-semiconductor field-effect transistors. They predicted that electrons may arrange into highly-correlated domains whose patterning shares similarity with microemulsions found in classical aqueous systems [9–11].

In Rashba spin-orbit coupled (SOC) Bose-Einstein condensates (BEC), a quantum "spin" microemulsion analogue was recently observed in finite-temperature numerical simulations [12]. In the spin microemulsion, atoms segregate based on pseudospin into isotropic domains resembling classical bicontinuous microemulsions [13]. Rashba SOC involves an isotropic two-dimensional coupling of momentum and (pseudo)spin [14–17], yielding a circular manifold of degenerate single-particle ground states. Our previous work [12] demonstrated how a superfluid stripe phase will melt above a critical temperature into this normal but highly spin-correlated microemulsion state, characterized by a circular, thermally broadened momentum distribution.

Although one-dimensional spin-momentum coupling cold atom experiments have become routine [18–21], accessing a genuinely isotropic 2D SOC is missing from modern SOC cold-atom experiments. Yet, significant theoretical interest [22–29] and experimental proposals [30–34] for studying Rashba bosons in cold atom experiments are mounting, with a recent experiment from the NIST group achieving a Rashba-like dispersion [35]. This suggests that Rashba SOC with a circular dispersion will soon be realized in cold-atom systems, and likely the novel quantum microemulsion state as well.

To aid the first experimental realization of the spin microemulsion phase, this study provides a comprehensive characterization of its thermodynamic stability, determined via equilibrium finite temperature simulations that embed full thermal and quantum fluctuation effects [36, 37]. In particular, we answer questions left by our previous work regarding the microemulsion's existence in miscible pseudospin condensates and slightly anisotropic SOC cases. We further explore the effect of a pseudospin population imbalance and determine a stable range in which the microemulsion state exists. Lastly, we highlight the microemulsion's robust thermodynamic stability in simulations with a harmonic trap, which mimics realistic experimental conditions.

II. METHODS

We consider ensembles of interacting pseudospin-1/2 Bose-Einstein condensates in two dimensions, described by a one-body Rashba Hamiltonian in the pseudospin

* ghf@ucsb.edu

basis

$$\hat{\underline{\underline{h}}} = \frac{1}{2m}(\hat{\mathbf{p}}\underline{\underline{I}} - \boldsymbol{\mathcal{A}})^2 + [U_{\text{ext}}(\mathbf{r}) - \mu]\underline{\underline{I}} + \frac{\hbar\delta}{2}\underline{\underline{\sigma}}^z, \quad (1)$$

where $\hat{\mathbf{p}}$ is the canonical momentum vector, m and μ are the atomic mass and chemical potential for both pseudospin components, δ describes a linear Zeeman shift achievable via a Raman laser detuning [18, 21], and $U_{\text{ext}}(\mathbf{r})$ describes a one-body external potential such as a harmonic trap or optical lattice. $\boldsymbol{\mathcal{A}} = \hbar\kappa(\underline{\underline{\sigma}}^x, \eta_\kappa\underline{\underline{\sigma}}^y)$ is a non-Abelian vector potential that incorporates a two-dimensional SOC of strength κ. We consider a simple model of the spin-orbit coupling anisotropy $\eta_\kappa \equiv \kappa_y/\kappa_x$, where $\eta_\kappa = 1$ represents the isotropic "Rashba" limit [26, 28]. $\underline{\underline{\sigma}}^\nu$ is the ν^{th} spin-1/2 Pauli matrix and $\underline{\underline{I}}$ is the 2×2 identity matrix.

For interacting pseudospin-1/2 BECs, we use the second-quantized Hamiltonian $\hat{H} = \int d^2r\, \hat{\Psi}^\dagger(\mathbf{r})\hat{\underline{\underline{h}}}\hat{\Psi}(\mathbf{r}) + \hat{H}_{\text{int}}$ where $\hat{\Psi}(\mathbf{r}) = (\hat{\psi}_\uparrow, \hat{\psi}_\downarrow)$ is a two-component vector of second-quantized field operators satisfying Bose commutation relations [38]. We assume the following contact interaction Hamiltonian

$$\hat{H}_{\text{int}} = \frac{1}{2}\sum_{\alpha\gamma}\int d^2r\, \hat{\psi}^\dagger_\alpha(\mathbf{r})\hat{\psi}^\dagger_\gamma(\mathbf{r})g_{\alpha\gamma}\hat{\psi}_\alpha(\mathbf{r})\hat{\psi}_\gamma(\mathbf{r}) \quad (2)$$

where $g_{\alpha\gamma}$ represents a repulsive coupling constant parametrizing the pairwise interaction between atoms in α and γ pseudospin states. We assume a symmetric matrix $g_{\uparrow\uparrow} = g_{\downarrow\downarrow} = g$ and $g_{\uparrow\downarrow} = g_{\downarrow\uparrow} = g\eta_g$, where η_g represents a miscibility parameter. The diagonal coupling constant g is parameterized by the s-wave scattering length a_s via $g = 4\pi\hbar^2 a_s/m$.

The spin microemulsion phase occurs at finite temperature [12] and thus requires beyond mean-field numerical treatment of the aforementioned model. To predict equilibrium phase behavior at finite temperature, we consider a grand canonical partition function $\mathcal{Z}(\mu, V, T) = \text{Tr}[e^{-\beta\hat{H}}]$ and use Feynmann's path-integral approach, discretizing the imaginary time interval $\tau \in [0, \beta]$, with $\beta = 1/k_B T$, into N_τ segments. The trace is conducted in a field-theoretic representation by choosing a basis of bosonic coherent state fields $(\phi_{\alpha,j}(\mathbf{r}), \phi^*_{\alpha,j}(\mathbf{r}))$ [39], which are a complex-conjugate pair of fields obeying periodic boundary conditions in imaginary time τ labeled with discrete index j.

The resulting field theory consists of functional integrals over coherent state fields $\mathcal{Z} = \int \mathcal{D}(\phi, \phi^*)e^{-S[\phi,\phi^*]}$ weighted by an action functional $S[\phi, \phi^*]$:

$$\begin{aligned} S[\phi,\phi^*] &= \sum_\alpha \sum_{j=0}^{N_\tau-1} \int d^2r\ \phi^*_{\alpha,j}(\mathbf{r})[\phi_{\alpha,j}(\mathbf{r}) - \phi_{\alpha,j-1}(\mathbf{r})] \\ &+ \frac{\beta}{N_\tau}\sum_{\alpha,\gamma}\sum_{j=0}^{N_\tau-1}\int d^2r\ \phi^*_{\alpha,j}(\mathbf{r})\,\hat{h}_{\alpha,\gamma}(\mathbf{r})\,\phi_{\gamma,j-1}(\mathbf{r}) \\ &+ \frac{\beta}{2N_\tau}\sum_{\alpha,\gamma}\sum_{j=0}^{N_\tau-1}\int d^2r\ \phi^*_{\alpha,j}(\mathbf{r})\phi^*_{\gamma,j}(\mathbf{r})g_{\alpha\gamma}\phi_{\gamma,j-1}(\mathbf{r})\phi_{\alpha,j-1}(\mathbf{r}). \end{aligned} \quad (3)$$

The complex-valued action presents a sign problem that hinders numerical sampling. We overcome that obstacle via the complex Langevin algorithm [36]

$$\begin{aligned} \frac{\partial}{\partial t}\phi_{\alpha,j}(\mathbf{r},t) &= -\frac{\delta S[\phi,\phi^*]}{\delta\phi^*_{\alpha,j}(\mathbf{r},t)} + \eta_{\alpha,j}(\mathbf{r},t) \\ \frac{\partial}{\partial t}\phi^*_{\alpha,j}(\mathbf{r},t) &= -\frac{\delta S[\phi,\phi^*]}{\delta\phi_{\alpha,j}(\mathbf{r},t)} + \eta^*_{\alpha,j}(\mathbf{r},t), \end{aligned} \quad (4)$$

where we have discretized the fields in space and imaginary time, indexed by j, and Gaussian white noises are built from real noise fields $\eta_{\alpha,j} = \eta^{(1)}_{\alpha,j} + i\eta^{(2)}_{\alpha,j}$ and $\eta^*_{\alpha,j} = \eta^{(1)}_{\alpha,j} - i\eta^{(2)}_{\alpha,j}$, where $\langle\eta^{(\mu)}_{\alpha,j}(\mathbf{r},t)\rangle = 0$ and $\langle\eta^{(\mu)}_{\alpha,j}(\mathbf{r},t)\eta^{(\nu)}_{\beta,k}(\mathbf{r}',t')\rangle = \delta_{\mu,\nu}\delta_{\alpha,\beta}\delta_{j,k}\delta(\mathbf{r}-\mathbf{r}')\delta(t-t')$. The complex Langevin algorithm entails evolving a coupled scheme of stochastic differential equations forward in fictitious time t; to accomplish this, we use an exponential-time-differencing algorithm [36] with adaptive time stepping [40]. Expressions for the action's functional derivatives are derived analytically in the conjugate wavevector - Matsubara frequency Fourier representation and subsequently evaluated via a pseudospectral implementation at each Langevin time step [37]. Additionally, the noise sources are $(d+1)$-Fourier transformed at each Langevin time step [36]. It can been shown that long-time, steady-state field trajectories will capture unbiased thermodynamics at finite temperature [41, 42].

Ensemble averaged thermodynamic observables are calculated via long Langevin-time averages of field-operator functionals of coherent state fields $\langle O\rangle = \frac{1}{N_{\text{CL}}}\sum_{n=1}^{N_{\text{CL}}}\tilde{O}[\boldsymbol{\phi}_n, \boldsymbol{\phi}^*_n]$ from N_{CL} decorrelated samples. To identify equilibrated phases, density snapshots $\tilde{\rho}_\alpha(\mathbf{r}) = 1/N_\tau\sum_{j=0}^{N_\tau-1}\phi^*_{\alpha,j}(\mathbf{r})\phi_{\alpha,j-1}(\mathbf{r})$ or thermal averages of the momentum distribution field operator $\tilde{N}_\mathbf{k} = A/N_\tau\sum_\alpha\sum_{j=0}^{N_\tau-1}\phi^*_{\alpha,-\mathbf{k}}\phi_{\alpha,\mathbf{k}}$ are analyzed, where $A = L_xL_y$ is the system area and $\mathbf{k}$ is a discrete wavevector used in Fourier collocation $\mathbf{k} = (2\pi/L)(n_x, n_y)$. We utilize square simulation cells $L_x = L_y = L$ discretized by N_x and N_y integer points in the $\hat{x}$ and $\hat{y}$ directions.

In bulk simulations ($U_{\text{ext}}(\mathbf{r}) = 0$), the superfluid density tensor is determined by the phase-twist method [12, 43], which quantifies the superfluid density tensor as a response coefficient of the thermodynamic grand potential to a small superflow. This leads to a relation where

the normal fluid density is quantified by the variance of the total physical momentum and then subtracted from the total density

$$\rho_{\rm SF}^{\mu\nu} = \delta_{\mu\nu}\langle N\rangle/A - (\beta/mA)[\langle P_\mu P_\nu\rangle - \langle P_\mu\rangle\langle P_\nu\rangle]. \quad (5)$$

The total particle number is computed by spatial integration of the density field operator $\tilde{N}[\boldsymbol{\phi},\boldsymbol{\phi}^*] \equiv \sum_\alpha \int d^2r \tilde{\rho}_\alpha(\mathbf{r})$, and the physical momentum field operator is computed via $\tilde{P}_\nu[\boldsymbol{\phi},\boldsymbol{\phi}^*] = 1/N_\tau \sum_{j=0}^{N_\tau-1}\sum_{\alpha\gamma}\int d^2r\ \phi^*_{\alpha,j}(\mathbf{r})(\hat{p}_\nu \underline{\underline{I}} - \mathcal{A}_\nu)_{\alpha\gamma}\phi_{\gamma,j-1}(\mathbf{r})$, where $(\hat{p}_\nu \underline{\underline{I}} - \mathcal{A}_\nu)_{\alpha\gamma}$ represents a matrix element of the physical momentum operator in the ν direction.

III. RESULTS

We investigate the necessary conditions to achieve the spin microemulsion in cold atomic gases. Previous results imply a requirement of Rashba (2D isotropic) SOC ($\eta_\kappa = 1$) as well as immiscible conditions ($\eta_g > 1$) [12], where the spin-segregated microemulsion-like domains share similar features to the stripe phase found in immiscible Rashba spin-orbit coupled BECs. To investigate these questions, we consider the trap-free "bulk" case ($U_{\rm ext}(\mathbf{r}) = 0$). In this scenario, the natural length scale is proportional to the BEC healing length $\ell = (\hbar^2/2m\mu_{\rm eff})^{1/2}$ [44], and we rescale the theory using this length scale. Taking $\mu_{\rm eff} \equiv \mu - \hbar^2\kappa^2(1+\eta_\kappa^2)/2m$ as the appropriate energy scale, we arrive at a dimensionless model parameterized by $\bar{T} = k_B T/\mu_{\rm eff}$, $\bar{\kappa} = \kappa\ell$, $\bar{g} = g2m/\hbar^2$, $\bar{\delta} \equiv \hbar\delta/2\mu_{\rm eff}$ as well as η_g and η_κ defined previously. We use $\bar{\delta}$ to investigate the effect of asymmetric pseudospin populations on the microemulsion state.

A. Spin-orbit Coupling Anisotropy

Creating a genuinely isotropic SOC in cold atom experiments presents the most significant hurdle in realizing the spin microemulsion. Early proposals were dominated by tripod and tetrapod schemes [31, 34, 45–47], which were later superceded by more controllable schemes [30, 48]. In the recent NIST experiment that implemented a Rashba-like SOC [35], they observed three degenerate minima instead of a ring in the single-particle spectrum because of Dresselhaus-like cubic and quadratic contributions. As this case suggests, the precise SOC anisotropy will depend on the particular experimental setup and choices therein, so we turn to a simple but well-established model [16, 26, 32, 48, 49] for SOC anisotropy in the Rashba Hamiltonian via $\eta_\kappa \equiv \kappa_y/\kappa_x$.

The specific question addressed is how much anisotropy in the SOC scheme is tolerated by the microemulsion before losing thermodynamic stability. To answer this question, we compute a phase diagram in the $\bar{T} - \eta_\kappa$ plane, shown in Figure (1). Via immiscible conditions ($\eta_g > 1$), we use a $\hat{x}$-modulated spin stripe ground state to study the effects of SOC anisotropy and thermal fluctuations. At $\eta_\kappa = 0$, the spin-orbit coupling scheme is effectively uniaxial and can be spin-rotated to correspond with the Rashba-Dresselhaus form at low Rabi coupling strength. Such a model has been implemented in many cold-atom SOC experiments to date [21]. When considering 2D SOC schemes at the single-particle level, increasing η_κ towards unity transforms the double-well minima at $\mathbf{k} = (\pm\bar{\kappa}, 0)$ to a degenerate circle of energy minima at $|\mathbf{k}| = \bar{\kappa}$.

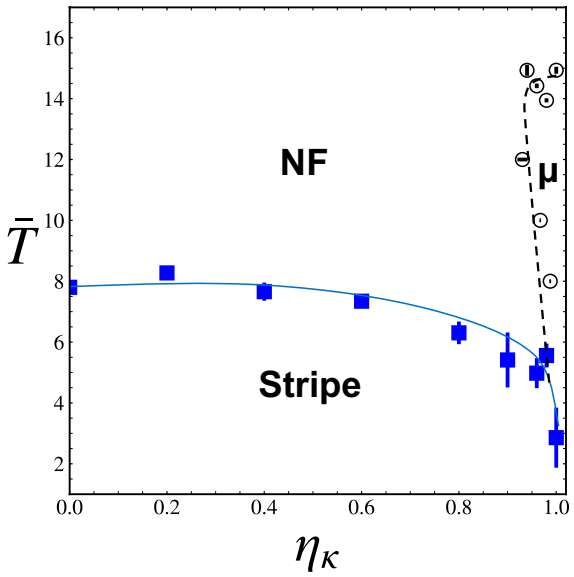

FIG. 1. Finite temperature phase diagram in the $\bar{T}$–η_κ plane, depicting the appearance of a microemulsion ($\boldsymbol{\mu}$) near isotropic conditions ($\eta_\kappa \to 1$), computed at $\eta_g = 1.2$, $\bar{g} = 0.075$, and $\bar{\kappa} = 0.6$. The blue squares denote a Kosterlitz–Thouless-like critical transition, while the open black circles denote the spin microemulsion to normal fluid (**NF**) crossover. The corresponding solid blue curve and dashed black curve serve as guides for the eye. Precise phase boundary points and their

error bars are determined in the Supplementary Material.

As η_κ increases, the superfluid critical transition temperature decreases, reflecting the diminished cost of pseudospin defects in the direction parallel to the stripes (orthogonal to the condensates' momenta). We determine the superfluid - normal fluid transition via a finite-size analysis on the stripe's superfluid density, which is detailed in the Supplementary Material. The shape of the superfluid-normal fluid transition curve shows qualitative agreement with previous analytical work [50]; however, our simulations provide numerical evidence for a microemulsion analogue phase appearing at $\eta_\kappa > 0.93$.

The boundary between the microemulsion and the normal fluid is a continuous crossover. Similar to previous work [12], we determine the microemulsion to normal fluid crossover temperature at constant η_κ by quantifying the ratio of the $\mathbf{k} = \mathbf{0}$ occupation to the most pop-

ulated mode $\langle N_{\mathbf{k}=\mathbf{0}}\rangle/\langle \max_{\mathbf{k}} N_{\mathbf{k}}\rangle$, which quantifies homogeneity in the Bose fields. At constant temperature, we determine a precise crossover η_κ value by varying η_κ and monitoring the anisotropy γ of the resulting momentum distribution $N_{\mathbf{k}}$, quantified by $\gamma = 1 - N_{\mathbf{k}=(0,\kappa)}/N_{\mathbf{k}=(\kappa,0)}$ via our prior definition for the momentum occupation. We discuss our determination of the crossover boundaries in detail in the Supplementary Material.

Figure (1) confirms the necessity of nearly isotropic spin-orbit coupling with many closely spaced single-particle states to produce a spin microemulsion. However, a perfectly isotropic SOC ($\eta_\kappa = 1$) is not required. This finding agrees with a previous mean-field study on crystalline states found in dipolar BECs with Rashba spin-orbit coupling. [29]. In the slightly anisotropic case $\eta_\kappa \to 1^-$, thermal fluctuations induce the occupation of nearly degenerate but low-lying excited momentum states on the circle $|\mathbf{k}| = \bar{\kappa}$, leading to a microemulsion phase despite a lack of genuine isotropic SOC. Furthermore, the crossover η_κ values decrease weakly with increasing temperature, suggesting that the microemulsion state can tolerate more anisotropic SOC schemes at higher temperatures before crossing over to homogeneous normal fluid. Thus, thermal fluctuations stabilize the microemulsion phase and promote a tolerance of some anisotropy in the SOC scheme. While these results are encouraging for the spin microemulsion's experimental realization, our current model does not consider higher order spin-momentum coupling terms that may be present in some experimental schemes and lead to other sources of SOC anisotropy [35]. An exploration of those SOC schemes is deferred to a future study.

B. Pseudospin Miscibility

At low temperatures, $\eta_g < 1$ and $\eta_g > 1$ yield a plane-wave phase and stripe phase, respectively [32]. Figure (2) depicts the expected finite-temperature phase diagram within the $\bar{T} - \eta_g$ plane, demonstrating the prevalence of the microemulsion in both miscible and immiscible conditions. Tracking the average momentum distributions confirms the presence of four different phases: One peak at $|\mathbf{k}| = \bar{\kappa}$ corresponding to a plane-wave phase, two peaks at $\mathbf{k} = (\pm\bar{\kappa}, 0)$ corresponding to a stripe phase, a macroscopic occupation of the Rashba circle $|\mathbf{k}| = \bar{\kappa}$ corresponding to the microemulsion phase, and a normal fluid represented by a thermally broadened peak centered around $\mathbf{k} = \mathbf{0}$.

Our previous work [12] confirmed the microemulsion phase only for immiscible conditions, which could limit experiments to particular atoms and hyperfine state pairs when creating a pseudospin-1/2 system. Contrary to this implication, we find that the miscible plane-wave phase undergoes a similar transition into the microemulsion at elevated temperature. While the plane-wave phase differs from the stripe phase in its pseudospin ordering, both phases share anisotropic superfluid character at low temperatures with the implementation of Rashba SOC.

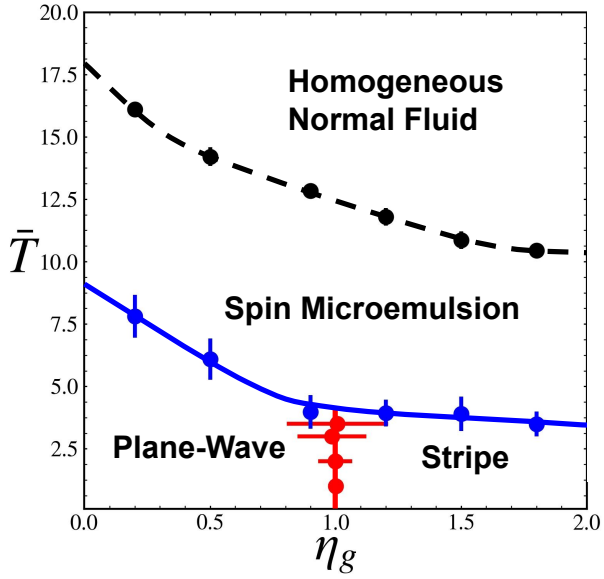

FIG. 2. We demonstrate the resilience of the microemulsion phase to miscibility effects via a phase diagram in the $\bar{T}$–η_g plane with $\bar{\kappa} = 0.6$, $\bar{g} = 0.1$, and $\eta_\kappa = 1.0$. $\eta_g < 1$ ($\eta_g > 1$) corresponds to the miscible (immiscible) case. Lines are a guide for the eye. The blue circles show a superfluid-microemulsion transition with Kosterlitz–Thouless-like character. The black dashed line represents a continuous crossover between spin microemulsion and homogeneous normal fluid. The red solid line denotes a first-order phase transition between the plane-wave and stripe phases. A discussion of error determination can be found in the Supplementary Material.

Using $\hat{x}$-oriented plane-wave and stripe initial conditions in Langevin sampling, we see a full decline in ρ^{xx}_{SF} near the melting temperature with Kosterlitz Thouless-like behavior [51]. To determine a precise critical temperature, we conduct a finite-size analysis in the Supplementary Material which incorporates a modified Kosterlitz–Thouless universal jump [43, 50, 52–54]. Our analysis suggests that the plane-wave and stripe phase undergo a Kosterlitz–Thouless-like transition with a similarly modified universal jump magnitude, which suggests a transition mediated by thermally-driven proliferation of half-vortex spin defects. A more detailed analysis of the simultaneous pseudospin and superfluid phase defects and their role in this transition is left for a future study.

Similar to Figure (1), we characterize the microemulsion to normal fluid crossover by tracking $\langle N_{\mathbf{k}=\mathbf{0}}\rangle/\langle \max_{\mathbf{k}} N_{\mathbf{k}}\rangle$. As we decrease miscibility (increase η_g), the repulsive energy scale increases at fixed chemical potential and lowers the critical temperature, resulting in a downward-sloping curve. At constant temperature, an increase in the repulsive energy scale disrupts the quantum character of the microemulsion and leads to a homogeneous normal fluid as atoms scatter into higher-energy momentum states.

When $\eta_g = 1.0$ at low temperatures, we observe a plane-wave to stripe first-order transition. First-order character is demonstrated by a kink in the grand potential Ω – the relevant thermodynamic potential in the grand canonical ensemble. Furthermore, we compute an integrated $\hat{x}$-magnetization via the corresponding field operator $\tilde{M}_x[\boldsymbol{\phi}, \boldsymbol{\phi}^*] = 1/N_\tau \sum_{\alpha\gamma} \sum_{j=0}^{N_\tau - 1} \int d^2r\, \phi^*_{\alpha,j}(\mathbf{r}) \sigma^x_{\alpha\gamma} \phi_{\gamma,j-1}(\mathbf{r})$ and observe a jump in the thermal-averaged $\hat{x}$-magnetization from non-zero in the spin-polarized plane-wave phase to 0 in the stripe phase; details are shown in the Supplementary Material [55]. We further distinguish this transition by the sharp peak in magnetic susceptibility $\chi_{xx} = \langle M_x^2 \rangle - \langle M_x \rangle^2$, which highlights the contribution of pseudospin fluctuations in the order-order transition. Our findings support the mean-field result, that the quantum phase transition occurs at $\eta_g = 1.0$ [56]. While the diagram suggests a tricritical point at $\eta_g = 1.0$, $\bar{T} = 3.8$, between plane-wave, stripe, and microemulsion phases, we defer a detailed investigation of that point's character to future work.

C. Imbalanced Pseudospin Mixtures

Next, we consider a microemulsion phase in bulk conditions where the mass fractions of atoms in the $|\uparrow\rangle$ and $|\downarrow\rangle$ states are imbalanced. To investigate within the present grand canonical formalism, we vary the dimensionless linear Zeeman shift strength $\bar{\delta}$, which explicitly breaks the system's time-reversal symmetry and the pseudospin population symmetry. This linear Zeeman shift parameter provides a symmetric way of adjusting the chemical potential imbalance between atoms in the $|\uparrow\rangle$ and $|\downarrow\rangle$ states. Such a linear Zeeman shift is typically controlled by the Raman laser detuning in cold-atom SOC experiments [18, 21]. Previous work [12] considered only equimolar mixtures ($\bar{\delta} = 0$), leaving an open question regarding the microemulsion's fate in pseudospin-polarized ensembles.

Starting with a microemulsion phase at $\bar{\delta} = 0$, we vary the linear Zeeman shift $\bar{\delta}$ at constant $\bar{T}$ in Figure (3) to study the conditions at which the microemulsion loses thermodynamic stability. As we vary $\bar{\delta}$, we determine the mass fraction of $|\downarrow\rangle$ via $\langle N_\downarrow \rangle / \langle N \rangle$ and record the corresponding superfluid and $\mathbf{k} = \mathbf{0}$ occupation fractions as the mass fraction changes. We additionally monitor the momentum distribution $N_\mathbf{k}$ to distinguish between the microemulsion, which has significant occupation in momentum states $|\mathbf{k}| = \bar{\kappa}$, and other competing phases.

Figure (3) demonstrates a wide range of thermodynamic stability for the microemulsion until the mass fraction exceeds $\sim 80\%$. At both temperatures considered, we find that the significant occupation of $|\mathbf{k}| = \bar{\kappa}$ momentum states disappears above a mass fraction of $\sim 80\%$, leaving a single condensed peak at $\mathbf{k} = \mathbf{0}$. This transition corresponds with the re-emergence of superfluidity and quasi-condensation above some critical Zeeman shift

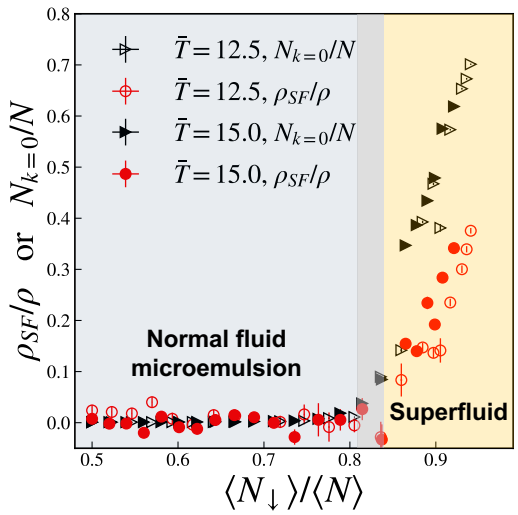

FIG. 3. Variation of pseudospin population imbalance, quantified by the $|\downarrow\rangle$ mass fraction $\langle N_\downarrow \rangle / \langle N \rangle$, for a spin microemulsion at $\bar{\kappa} = 0.75$, $\eta_g = 0.8$, $\bar{g} = 0.1$, $\eta_\kappa = 1$ in a box with dimensionless length $\bar{L} = 50.27$ at two different temperatures $\bar{T} = 12.5$ (empty markers) and $\bar{T} = 15$ (filled markers). $\mathbf{k} = \mathbf{0}$ total occupation fraction (black triangles) and superfluid fraction (circles) at both temperatures depict a transition between the normal fluid microemulsion and the homogeneous superfluid. Simulations were conducted with an imaginary time discretization $\Delta_\tau \equiv (\bar{T} N_\tau)^{-1} = 0.002$ and a 200×200 spatial grid.

value $\bar{\delta} > \bar{\delta}_c$, where a quasi-long range ordered fluid with power-law spatial correlations appears. The finite-sized nature of our simulations reflects experimental conditions which typically consider 10^3-10^7 atoms. Analysis of the single-particle spectrum $E_\pm(\mathbf{k})$ at non-zero $\bar{\delta}$ supports our finding of a homogeneous superfluid, where for $\bar{\delta} \gg 1$ the ring degeneracy disappears and leaves a single energy minimum at $\mathbf{k} = \mathbf{0}$.

D. Presence of a Trapping Potential

Finally, we demonstrate the feasibility of observing the microemulsion phase by simulating a representative ^{87}Rb BEC experiment. We consider a pseudospin-1/2 gas formed by isolating the $|F = 1, m_F = +1\rangle$ and $|F = 1, m_F = -1\rangle$ hyperfine states. We target $N \sim 6 \times 10^4$ atoms total by choosing $\mu_{\text{eff}} = \hbar \times 0.90 \times 2\pi$ kHz. For artificial spin-orbit coupling, we consider an isotropic scheme ($\eta_\kappa = 1$) and a Raman laser wavelength $\lambda_\text{R} = 804.1$ nm which corresponds to a spin-orbit coupling strength $\kappa = \sqrt{2}\pi/\lambda_\text{R} = 5.53\ \mu\text{m}^{-1}$ [18, 57, 58].

We emulate an effective isotropic two-dimensional environment by considering trapping frequencies $\boldsymbol{\omega} = (\omega_{2\text{D}}, \omega_{2\text{D}}, \omega_z) = (77, 77, 250) \times 2\pi$ Hz [35, 59]. Here we assume a harmonic, pseudospin-independent trapping potential $U_\text{ext}(\mathbf{r}) = m\omega_{2\text{D}}^2 \mathbf{r}^2/2$ and re-scale Equations (1)

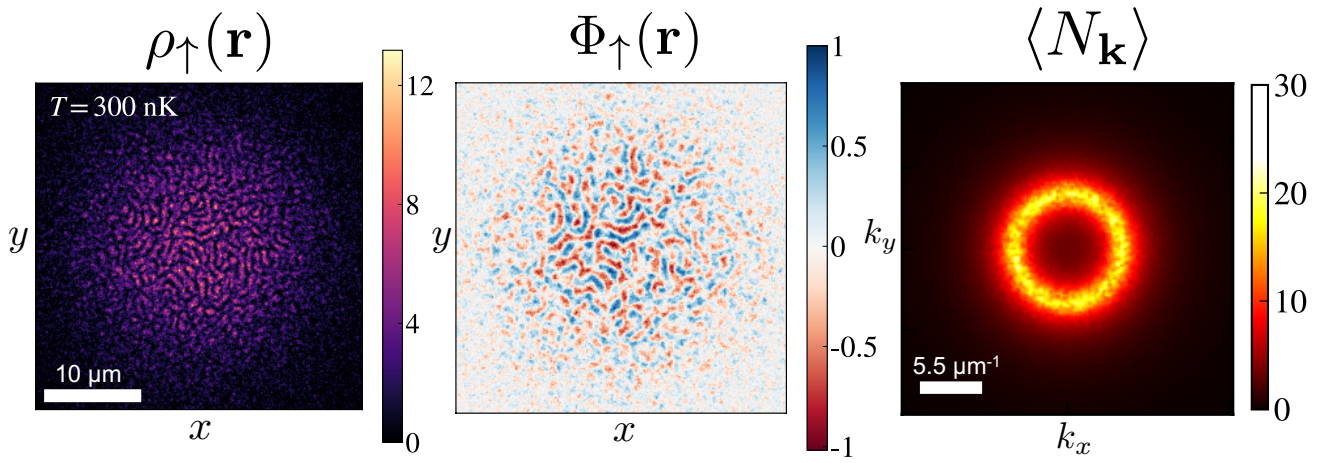

FIG. 4. Spin microemulsion appears in field-theoretic simulations of a trapped, Rashba-SOC ^{87}Rb BEC at $\bar{\mu} = 11.7$, $\bar{\kappa} = 6.79$, and $\bar{T} = 81.18$, which corresponds to approximately 300 [nK]. Snapshots of the a) density profile $\rho_\uparrow(\mathbf{r})$ and b) condensate wavefunction $\Phi_\uparrow(\mathbf{r})$ for atoms in the $|\uparrow\rangle$ pseudospin state, with the x and y axes in units of μm. (c) Thermal-averaged quasi-momentum distribution demonstrates the microemulsion's isotropic character, with the k_x and k_y axes in units of $(\mu\text{m})^{-1}$. The simulation was conducted in a 30 μm $\times$ 30 μm simulation cell using a 324×324 spatial grid and an imaginary time discretization of $\Delta_\tau \equiv (\bar{T}N_\tau)^{-1} = 5.1325 \times 10^{-4}$.

and (2) by the in-plane oscillator length $\ell_{2D} = \sqrt{\hbar/m\omega_{2D}}$ and oscillator energy $\hbar\omega_{2D}$. As a result, we recover an alternative dimensionless spin-orbit coupling strength $\bar{\kappa} = \kappa\ell_{2D}$ and temperature $\bar{T} = k_B T/\hbar\omega_{2D}$ hereafter and additionally introduce a dimensionless chemical potential $\bar{\mu} = \mu_{\text{eff}}/\hbar\omega_{2D}$. The dimensionless repulsion $\bar{g}$ and miscibility η_g retain their prior definitions.

Using the ^{87}Rb spinor scattering properties [60] $a_{F=0} = 101.8a_0$ and $a_{F=2} = 100.4a_0$ with a_0 the Bohr radius ($1a_0 = 0.529\mathring{A}$), we estimate the corresponding repulsive coupling constants $g_0 = 4\pi\hbar^2(a_{F=0} + 2a_{F=2})/3m$ and $g_2 = 4\pi\hbar^2(a_{F=2} - a_{F=0})/3m$. For the hyperfine states considered, this leads to symmetric intraspin and interspin coupling constants $g = g_{\uparrow\uparrow} = g_{\downarrow\downarrow} = g_0 + g_2$ and $g_{\uparrow\downarrow} = g_{\downarrow\uparrow} = g_0 - g_2$, such that Equation (2) is readily applicable. Considering a tight confinement in $\hat{z}$, we convert to a two-dimensional repulsive constant $g_{2D} = g/\sqrt{2\pi}\ell_z$ and take ℓ_{2D} as the natural length scale [58, 61]. We find $\bar{g} = 0.0781$ and $\eta_g = 1.0093$ appropriate for the $|1, 1\rangle$ and $|1, -1\rangle$ ^{87}Rb hyperfine mixture in this effective 2D environment.

We simulate the trapped Rashba-SOC BEC system using our field-theoretic complex Langevin formalism. Field-theoretic simulations uncover the spin microemulsion phase under confinement above $T_c \sim 250$ [nK]. Figure (4a) shows the density profile of $|\uparrow\rangle$ atoms in a spin microemulsion confined by an isotropic harmonic trap at $T = 300$ nK. Using the chemical potential specified above and no Zeeman shift ($\bar{\delta} = 0$), we observe an equal mixture of pseudospin states with $\langle N \rangle = 6.7 \times 10^4$ atoms total. We expect the microemulsion to emerge when $\bar{\kappa} > 1$ which corresponds to a much larger harmonic trap length scale compared to the SOC length scale that characterizes the microemulsion's domain widths.

Microemulsion-like domains appear in the center of the trap, while normal fluid appears on the system's edges. A corresponding snapshot of the condensate order parameter's spatial profile $\Phi_\alpha(\mathbf{r}) = 1/N_\tau \sum_{j=0}^{N_\tau - 1} \phi_{\alpha,j}(\mathbf{r})$ [37] is shown in Figure (4b) and confirms the presence of quantum correlations near the trap center despite the system's lack of superfluidity. Figure (4c) shows the circular quasi-momentum distribution characteristic of the isotropic spin microemulsion previously predicted in bulk systems [12]. Cold-atom experimental realizations of the spin microemulsion would observe this ring-shaped quasi-momentum distribution in time-of-flight measurements.

While the cloud diameter is estimated at approximately 14 μm, microemulsion domains in Figure (4a) have a width of ~ 0.6 μm, agreeing well with the expected characteristic length $\ell \sim \pi\kappa^{-1} = 0.57\mu$m in bulk, homogeneous conditions [12]. In the trapping and spin-orbit coupling conditions considered, we estimate the ratio of the SOC recoil energy $\hbar^2\kappa^2/2m$ to the in-plane oscillator energy as $\bar{\kappa}^2/2 = 23.05$. In this regime, the microemulsion state previously found in homogeneous conditions can readily emerge because of the dominating spin-orbit coupling and thermal energy scales.

IV. CONCLUSION

With experimental realization in mind, we have provided a survey of the spin-correlated microemulsion's thermodynamic stability using equilibrium, field-theoretic simulations of spin-orbit coupled pseudospin-1/2 Bose gases. Our results highlight the requirement of near isotropic Rashba spin-orbit coupling, necessary to achieve a circular manifold of degenerate or

nearly-degenerate single-particle states. Augmenting this single-particle intuition, we provide a phase diagram that demonstrates how the nature of the atomic repulsions, characterized by s-wave scattering lengths of hyperfine states, does not alter the character or presence of the spin microemulsion. As a result, there is flexibility in the choice of pseudospin states and atom in a potential experimental realization of the spin microemulsion. Furthermore, our simulations show that the spin microemulsion is robust to significant z-pseudospin-polarization and is not susceptible to slight imbalances in pseudospin state populations. Finally, we demonstrate the feasibility of realizing the spin microemulsion in experiments by simulating a representative ^{87}Rb experiment in an effective two-dimensional isotropic trap.

ACKNOWLEDGEMENTS

The authors thank David Weld for helpful discussions. This work was enabled by field-theoretic simulation tools developed under support from the National Science Foundation (CMMT Program, DMR-2104255). Use was made of computational facilities purchased with funds from the NSF (CNS-1725797) and administered by the Center for Scientific Computing (CSC). This work made use of the BioPACIFIC Materials Innovation Platform computing resources of the National Science Foundation Award No. DMR-1933487. The CSC is supported by the California NanoSystems Institute and the Materials Research Science and Engineering Center (MRSEC; NSF DMR 2308708) at UC Santa Barbara. E.C.M acknowledges support from a Mitsubishi Chemical Fellowship, and L.B. acknowledges support from the DOE, Office of Science, Basic Energy Sciences under Award No. DE-FG02-08ER46524.

[1] J. W. Harter, Z. Y. Zhao, J.-Q. Yan, D. G. Mandrus, and D. Hsieh, Science **356**, 295 (2017).
[2] L. Radzihovsky and A. Vishwanath, Physical Review Letters **103**, 010404 (2009).
[3] E. Fradkin and S. A. Kivelson, Physical Review B **59**, 8065 (1999).
[4] M. Zarenia, D. Neilson, and F. M. Peeters, Scientific Reports **7**, 11510 (2017).
[5] G. Schmid and M. Troyer, Physical Review Letters **93**, 067003 (2004).
[6] J.-R. Li, J. Lee, W. Huang, S. Burchesky, B. Shteynas, F. Ç. Top, A. O. Jamison, and W. Ketterle, Nature **543**, 91 (2017).
[7] B. Spivak and S. A. Kivelson, Physical Review B **70**, 155114 (2004).
[8] B. Spivak and S. A. Kivelson, Annals of Physics **321**, 2071 (2006).
[9] P. G. De Gennes and C. Taupin, The Journal of Physical Chemistry **86**, 2294 (1982).
[10] S. Guo, H. Tao, G. Gao, S. Mhatre, Y. Lu, A. Takagi, J. Li, L. Mo, O. J. Rojas, and G. Chu, Biomacromolecules **24**, 367 (2023).
[11] R. K. W. Spencer and M. W. Matsen, Macromolecules **54**, 1329 (2021).
[12] E. C. McGarrigle, K. T. Delaney, L. Balents, and G. H. Fredrickson, Physical Review Letters **131**, 173403 (2023).
[13] F. S. Bates, W. W. Maurer, P. M. Lipic, M. A. Hillmyer, K. Almdal, K. Mortensen, G. H. Fredrickson, and T. P. Lodge, Physical Review Letters **79**, 849 (1997).
[14] A. Manchon, H. C. Koo, J. Nitta, S. M. Frolov, and R. A. Duine, Nature Materials **14**, 871 (2015).
[15] Y. A. Bychkov and E. I. Rashba, Journal of Physics C: Solid State Physics **17**, 6039 (1984).
[16] T. D. Stanescu, B. Anderson, and V. Galitski, Physical Review A **78**, 023616 (2008).
[17] K. Wu, J. Chen, H. Ma, L. Wan, W. Hu, and J. Yang, Nano Letters **21**, 740 (2021).
[18] Y.-J. Lin, K. Jiménez-García, and I. B. Spielman, Nature **471**, 83 (2011).
[19] S.-C. Ji, J.-Y. Zhang, L. Zhang, Z.-D. Du, W. Zheng, Y.-J. Deng, H. Zhai, S. Chen, and J.-W. Pan, Nature Physics **10**, 314 (2014).
[20] T. M. Bersano, J. Hou, S. Mossman, V. Gokhroo, X.-W. Luo, K. Sun, C. Zhang, and P. Engels, Physical Review A **99**, 051602 (2019).
[21] Y. Zhang, M. E. Mossman, T. Busch, P. Engels, and C. Zhang, Frontiers of Physics **11**, 118103 (2016).
[22] T. A. Sedrakyan, A. Kamenev, and L. I. Glazman, Physical Review A **86**, 063639 (2012).
[23] T. A. Sedrakyan, V. M. Galitski, and A. Kamenev, Physical Review Letters **115**, 195301 (2015).
[24] S. Sinha, R. Nath, and L. Santos, Physical Review Letters **107**, 270401 (2011).
[25] S. Sur and K. Yang, Physical Review B **100**, 024519 (2019).
[26] E. Kawasaki and M. Holzmann, Physical Review A **95**, 051601 (2017).
[27] T. Ozawa and G. Baym, Physical Review Letters **110**, 085304 (2013).
[28] J. Radić, A. Di Ciolo, K. Sun, and V. Galitski, Physical Review Letters **109**, 085303 (2012).
[29] S. Gopalakrishnan, I. Martin, and E. A. Demler, Physical Review Letters **111**, 185304 (2013).
[30] D. L. Campbell and I. B. Spielman, New Journal of Physics **18**, 033035 (2016).
[31] J. Ruseckas, G. Juzeliūnas, P. Öhberg, and M. Fleischhauer, Physical Review Letters **95**, 010404 (2005).

[32] N. Goldman, G. Juzeliūnas, P. Öhberg, and I. B. Spielman, Reports on Progress in Physics **77**, 126401 (2014).

[33] D. L. Campbell, G. Juzeliūnas, and I. B. Spielman, Physical Review A **84**, 025602 (2011).

[34] G. Juzeliūnas, J. Ruseckas, and J. Dalibard, Physical Review A **81**, 053403 (2010).

[35] A. Valdés-Curiel, D. Trypogeorgos, Q.-Y. Liang, R. P. Anderson, and I. B. Spielman, Nature Communications **12**, 593 (2021).

[36] K. T. Delaney, H. Orland, and G. H. Fredrickson, Physical Review Letters **124**, 070601 (2020).

[37] G. H. Fredrickson, K. T. Delaney, G. H. Fredrickson, and K. T. Delaney, *Field-Theoretic Simulations in Soft Matter and Quantum Fluids*, International Series of Monographs on Physics (Oxford University Press, Oxford, New York, 2023).

[38] A. L. Fetter and J. D. Walecka, *Quantum Theory of Many-Particle Systems* (Courier Corporation, 2012).

[39] J. W. Negele and H. Orland, *Quantum Many-particle Systems* (Basic Books, 1988).

[40] G. Aarts, F. A. James, E. Seiler, and I.-O. Stamatescu, Physics Letters B **687**, 154 (2010), arxiv:0912.0617.

[41] G. Parisi, Physics Letters B **131**, 393 (1983).

[42] J. R. Klauder, Journal of Physics A: Mathematical and General **16**, L317 (1983).

[43] A. L. Subaşı and M. Iskin, Physical Review A **105**, 023301 (2022).

[44] L. Pitaevskii and S. Stringari, *Bose-Einstein Condensation and Superfluidity* (Oxford University Press, 2016).

[45] J. Dalibard, F. Gerbier, G. Juzeliūnas, and P. Öhberg, Reviews of Modern Physics **83**, 1523 (2011).

[46] X.-J. Liu, M. F. Borunda, X. Liu, and J. Sinova, Physical Review Letters **102**, 046402 (2009).

[47] S.-L. Zhu, H. Fu, C.-J. Wu, S.-C. Zhang, and L.-M. Duan, Physical Review Letters **97**, 240401 (2006).

[48] L. Huang, Z. Meng, P. Wang, P. Peng, S.-L. Zhang, L. Chen, D. Li, Q. Zhou, and J. Zhang, Nature Physics **12**, 540 (2016).

[49] S.-W. Su, I.-K. Liu, S.-C. Gou, R. Liao, O. Fialko, and J. Brand, Physical Review A **95**, 053629 (2017).

[50] C.-M. Jian and H. Zhai, Physical Review B **84**, 060508 (2011).

[51] D. R. Nelson and J. M. Kosterlitz, Physical Review Letters **39**, 1201 (1977).

[52] R. Bombín, F. Mazzanti, and J. Boronat, Physical Review A **100**, 063614 (2019).

[53] M. Kobayashi, M. Eto, and M. Nitta, Physical Review Letters **123**, 075303 (2019).

[54] C. Hickey and A. Paramekanti, Physical Review Letters **113**, 265302 (2014).

[55] G. H. Fredrickson and K. T. Delaney, Proceedings of the National Academy of Sciences **119**, e2201804119 (2022).

[56] R. Liao, Physical Review Letters **120**, 140403 (2018).

[57] G. I. Martone, Y. Li, and S. Stringari, Physical Review A **90**, 041604 (2014).

[58] K. T. Geier, G. I. Martone, P. Hauke, and S. Stringari, Physical Review Letters **127**, 115301 (2021).

[59] T. Yefsah, R. Desbuquois, L. Chomaz, K. J. Günter, and J. Dalibard, Physical Review Letters **107**, 130401 (2011).

[60] E. G. M. van Kempen, S. J. J. M. F. Kokkelmans, D. J. Heinzen, and B. J. Verhaar, Physical Review Letters **88**, 093201 (2002).

[61] K. T. Geier, G. I. Martone, P. Hauke, W. Ketterle, and S. Stringari, Physical Review Letters **130**, 156001 (2023).